Numerical Simulation of Intensity and Phase Noise From Extracted Parameters for CW DFB Lasers

Irshaad Fatadin, *Member, IEEE*, David Ives, and Martin Wicks

***Abstract*—A self-consistent numerical approach is demonstrated to analyze intensity and phase noise from experimentally extracted parameters for a continuous-wave distributed feedback (DFB) laser. The approach takes into account the intrinsic fluctuations of the photon number, carrier number, and phase. Values for the parameters appearing in the rate equations are extracted from the measured relative intensity noise spectra and linewidth of the laser. The simulation of the frequency spectra of intensity and phase noise of the DFB laser are performed by fast Fourier transform and exhibit good agreement with experimental results. The model presented here can readily be extended for the purpose of system simulations.**

***Index Terms*—Noise, numerical simulation, parameter extraction, rate equations, semiconductor lasers.**

I. Introduction

LIGHTWAVE systems, based on directly modulated distributed feedback (DFB) lasers, operate at bit rates up to 10 Gb/s [1], [2]. Accurate simulation of these systems requires numerical models of the individual components used. Such a model must be consistent with the measured properties of the component while predicting system performance beyond that possible from these basic measurements. The DFB laser is one important component that requires such a numerical model in order to help predict its dynamic properties.

Laser intensity noise [3]–[5] is one of the main factors limiting the dynamic range of laser-based lightwave systems. Wavelength modulation (frequency noise or chirp) may result in dispersion penalties, especially in long distance optical links. Analysis of the laser noise-types is necessary for further improvement of device and system performance.

In this paper, computer simulation based on direct numerical integration of the laser rate equations, including the effect of Langevin noise sources, is discussed using extracted parameters for a DFB laser. We propose measurement techniques for extracting the parameters of the laser that involve simple data manipulation and curve fitting to the measured relative intensity noise (RIN) spectra and linewidth of the laser. The paper is organized as follows. The laser diode rate-equation model, including noise fluctuations, is introduced in the next section. Section III outlines the measurements performed to obtain the RIN spectra and linewidth of the laser. The basic formalism used in the extraction procedure is given and the parameters obtained for the DFB laser are presented. In Section IV, we report the results of the numerical model to analyze the intensity and phase noise, and broadening of the line shape taking into account the correlations of the noise sources. The frequency spectra of both intensity and phase noise are calculated by fast Fourier transform (FFT) and the simulated data are compared with measurements. Finally, we draw conclusions from our work in Section V.

Manuscript received November 2, 2005; revised May 18, 2006. This work was supported in part by the Department of Trade and Industry's National Measurement System Directorate (NMSD) under Contract GBBK/C/11/12.

The authors are with the National Physical Laboratory, Teddington, Middlesex TW11 0LW, U.K. (e-mail: irshaad.fatadin@npl.co.uk; david.ives@npl.co.uk; martin.wicks@npl.co.uk).

Digital Object Identifier 10.1109/JQE.2006.880117

II. Laser Diode Rate-Equation Model

The laser dynamics are modelled by coupled rate equations [6], driven by noise sources, $F_i(t)$, which describe the relation between the carrier number $N(t)$, photon number $S(t)$, and optical phase $\theta(t)$

$$\frac{dN(t)}{dt} = \frac{I(t)}{q} - \frac{N(t)}{\tau_n} - g\frac{N(t)-N_0}{1+\epsilon S(t)}S(t) + F_N(t) \quad (1)$$

$$\frac{dS(t)}{dt} = g\frac{N(t)-N_0}{1+\epsilon S(t)}S(t) - \frac{S(t)}{\tau_p} + \frac{\beta N(t)}{\tau_n} + F_S(t) \quad (2)$$

$$\frac{d\theta(t)}{dt} = \frac{\alpha}{2}g\left(N(t)-\bar{N}\right) + F_\theta(t) \quad (3)$$

where $I(t)$ is the injected current, q is the electron charge, τ_n is the carrier lifetime, τ_p is the photon lifetime, g is the gain slope constant coefficient, ϵ is the nonlinear gain compression factor, N_0 is the carrier number at transparency, β is the fraction of spontaneous emission coupled into the lasing mode, α is the linewidth enhancement factor, and $\bar{N}$ is the time-averaged carrier number. The coupling strength of the grating in the DFB laser, usually expressed as the product of the coupling coefficient and the laser length, determines the cavity loss and hence the photon lifetime τ_p [7].

In the rate equations used here, the diffusion [8] and nonlinear effects [9] are lumped together as an effective field-dependent optical gain compression. This rather simple form is commonly employed by many authors [6], [10]–[12], although the gain compression term, $1/(1+\epsilon S)$, may also appear as $(1-\epsilon S)$ or $1/(1+\epsilon S)^{1/2}$ [13], [14]. According to [15], the form $1/(1+\epsilon S)$ agrees best with numerical solutions using more detailed models even for large photon densities. For small photon densities all forms are nearly identical. Optical feedback into the laser [16] is not accounted for by this model. However, optical feedback can be reduced experimentally by sufficient optical isolation.

The fluctuation of the lasing frequency $\Delta\nu(t)$ is described by the variation of the optical phase as

$$\Delta\nu(t) = \frac{1}{2\pi}\frac{d\theta}{dt}. \quad (4)$$

The random noise functions in (1)–(3) are assumed to be Gaussian random variables representing the Langevin noise sources related to carriers, photons, and phase, respectively. Under the Markovian assumption, the Langevin forces satisfy the general relations [17]

$$\langle F_i(t)\rangle = 0 \tag{5}$$

$$\langle F_i(t)F_j(t')\rangle = 2D_{ij}\delta(t-t') \tag{6}$$

where δ is Dirac's delta function and D_{ij} is the diffusion coefficient associated with the corresponding noise source defined as [17], [18]

$$2D_{\rm SS} = \frac{2\beta N(t)S(t)}{\tau_n} \tag{7}$$

$$2D_{NN} = \frac{2N(t)}{\tau_n}\left[1+\beta S(t)\right] \tag{8}$$

$$2D_{\theta\theta} = \frac{\beta N(t)}{2\tau_n S(t)} \tag{9}$$

$$2D_{SN} = \frac{-2\beta N(t)S(t)}{\tau_n} \tag{10}$$

$$2D_{S\theta} = 0 \tag{11}$$

$$2D_{N\theta} = 0. \tag{12}$$

The output optical power is given by

$$P(t) = \eta_d \frac{h\nu}{\tau_p} S(t) \tag{13}$$

where η_d is the differential quantum efficiency, h is Planck's constant, and ν is the unmodulated optical frequency. The threshold current of the DFB laser is expressed as

$$I_{\rm th} = \frac{q}{\tau_n}\left[N_o + \frac{1}{g\tau_p}\right]. \tag{14}$$

III. Parameter Extraction Procedure

A. Outline of the Process

The parameter extraction for the continuous-wave (CW) DFB laser was performed by measuring the RIN spectra for a number of injection current levels. These spectra were fitted to obtain values for g, τ_n, τ_p, ϵ, β, and N_0 appearing in (1)–(3). The output optical power emitted from the fiber pigtail was measured as a function of laser current to obtain the slope efficiency and calculate η_d in (13). Finally, the linewidth of the DFB laser was measured using the homodyne measurement technique [19] to estimate the linewidth enhancement factor α.

B. RIN Measurements

The experimental arrangement for measuring the RIN spectra of the laser source is shown in Fig. 1. The DFB laser is a commercially available fiber pigtailed butterfly package. An optical isolator integrated within this package avoids perturbation caused by optical feedback into the laser cavity. The laser is designed for direct modulation at 2.5 Gb/s with low chirp suitable for metro wavelength-division multiplexing (WDM) systems up to 100 km. The temperature of the DFB laser under test was set by the temperature controller module and a constant current driver source provides the laser injection current, I. The optical output was passed through a variable optical attenuator before being detected by the avalanche-photodiode field-effect transistor (APD-FET) receiver. The electrical spectrum analyzer (ESA) displays the electrical noise power spectrum which is proportional to the optical noise power squared. The RIN is defined as [20]

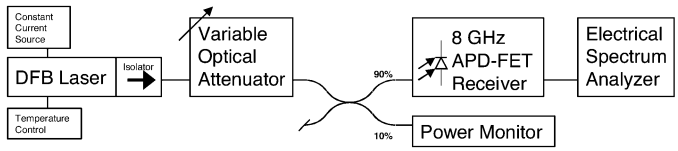

Fig. 1. Experimental arrangement for the RIN measurements.

$$\mathrm{RIN}(\omega) = \frac{\langle \delta P(\omega)^2\rangle}{\langle P\rangle^2} \tag{15}$$

where $\langle \delta P(\omega)^2\rangle$ is the mean square intensity-fluctuation spectral density of the optical signal and $\langle P\rangle$ is the average optical power.

The noise spectra were measured for ten different laser injection currents ranging from 1.3 to 3.0 times the threshold current. These noise spectra include the RIN from the laser under test, shot noise and thermal noise from the measurement system. The combined shot and thermal noise was measured by driving the laser hard (six times threshold). The optical attenuator was adjusted to maintain the same optical power level at the power monitor. For this injection current level, the RIN from the laser was found to be negligible. The thermal noise, which includes the contributions from the detector, amplifier and the ESA, was measured by turning the laser off.

The measured RIN spectra were derived from the measured noise spectra by first subtracting the shot and thermal noise and then normalizing the curves to the shot noise to remove the spectral response of the measurement system [21]. The overall calibration was achieved by measuring the RIN of a polarized and optically filtered erbium-doped fiber amplifier (EDFA) noise source [22], which can be related to its optical spectrum, to provide an estimate of the actual shot noise level. The measured RIN spectra of the DFB laser obtained for three different injection current levels are shown in Fig. 2.

C. Curve Fitting for Parameter Extraction

From small signal analysis of the laser rate equations it can be shown that the RIN spectrum has the analytical form given by

$$\mathrm{RIN}(\omega) = \frac{RZ^2(1+A\omega^2)}{Z^2+(Y^2-2Z)\omega^2+\omega^4} \tag{16}$$

where the curve parameters Y, Z, A, and R are functions of the injection current I and the laser parameters as expressed in

$$Y = \frac{1}{\tau_n} + \frac{1}{\tau_p} + \frac{g}{1+\epsilon S}\left[S - \frac{N-N_0}{1+\epsilon S}\right] \tag{17}$$

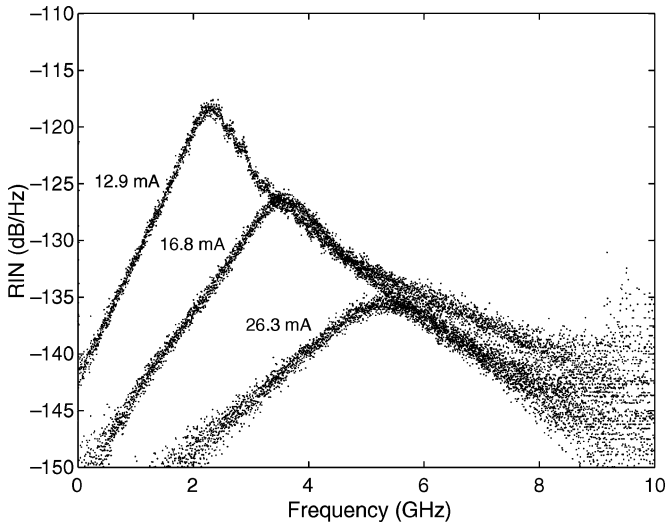

Fig. 2. Measured RIN spectra for three different injection currents.

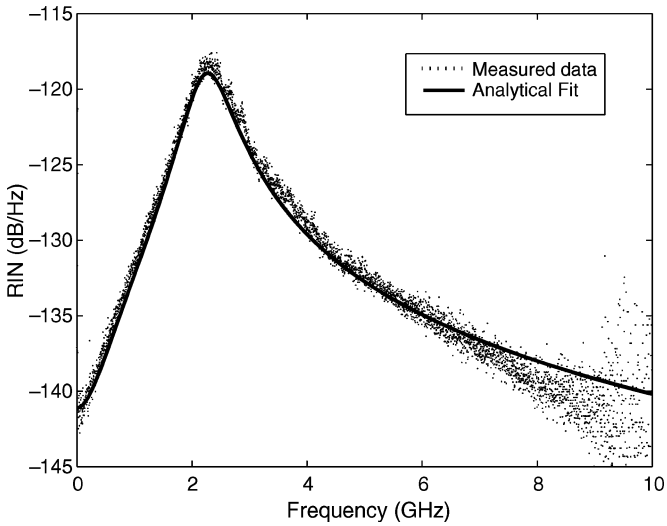

Fig. 3. Fitted analytical curve to the measured RIN spectrum at an injection current $I = 12.9$ mA.

$$Z = \frac{1}{\tau_n \tau_p} + \frac{g}{1+\epsilon S}\left[\frac{S}{\tau_p} - \frac{1-\beta}{\tau_n}\cdot\frac{N-N_0}{1+\epsilon S}\right] \tag{18}$$

$$A = \left\{\frac{1}{\tau_n^2}\left[(1-\beta)^2 + \frac{\beta}{S}\right] + \frac{g}{1+\epsilon S} \times \left[\frac{2}{\tau_n} + \frac{S}{\beta}\cdot\frac{g}{1+\epsilon S}\right]\right\}^{-1} \tag{19}$$

$$R = 2\tau_p^2(1+\epsilon S)^2 N \times \left[\frac{\beta\big(S(1-\beta)^2+\beta\big)(1+\epsilon S)^2 + gS\tau_n(gS\tau_n + 2\beta\epsilon S + 2\beta)}{S^2\tau_n\left(\tau_p g(1-\beta)(N-N_0) - (1+\epsilon S)\left(gS\tau_n + (1+\epsilon S)\right)\right)^2}\right]. \tag{20}$$

The curve parameters Y and Z represent the damping factor and the relaxation frequency of the DFB laser, respectively. The carrier number N and the photon number S were obtained by solving (1) and (2) for a given laser injection current I under steady state conditions. This gives the following solution for N:

$$N = \frac{\tau_n}{q}\cdot\frac{I(1+\epsilon S) + gN_0 qS}{1+\epsilon S + gS\tau_n} \tag{21}$$

which when substituted in (2) gives a quadratic in S. This has the usual solution

$$S = \frac{-b + \sqrt{b^2 - 4ac}}{2a} \tag{22}$$

where the negative root is unphysical, and

$$a = q(\epsilon + g\tau_n) \tag{23}$$

$$b = q + g\tau_p\left[(1-\beta)N_0 q - \tau_n I\right] - \beta\epsilon\tau_p I \tag{24}$$

$$c = -\beta\tau_p I. \tag{25}$$

The analytical expression (16) was used to fit the ten measured RIN spectra. The fitted curve to the RIN data at an injection current $I = 12.9$ mA is shown in Fig. 3. The laser parameters were extracted by minimizing the sum of squares of the differences between the ten analytical RIN spectra and the corresponding measured RIN spectra in the log domain. The data analysis was restricted to the frequency range 50 MHz to 8.0 GHz and for measured $\mathrm{RIN} > -145$ dB/Hz so that outliers would not adversely affect the result. The sum of squared errors was minimized over the variables by using an in-house modified Gauss–Newton algorithm. The optimization process is nonlinear and the initial estimates were chosen within reasonable bounds so that the minimization converged.

TABLE I
EXTRACTED PARAMETERS FOR DFB LASER RATE EQUATIONS

Parameter	Extracted Value
g ($\times 10^4$ s^{-1})	1.13
τ_n (ns)	0.33
τ_p (ps)	7.15
ϵ ($\times 10^{-8}$)	4.58
β ($\times 10^{-5}$)	3.54
N_0 ($\times 10^6$)	8.20
η_d	0.21

D. Resulting Extracted Parameters

The extracted parameters for the packaged DFB laser are given in Table I. The threshold current I_{th} is calculated from the extracted parameters of the laser using (14) and was found to be 10.0 mA compared to a measured value of 10.2 mA. The slight discrepancy can be attributed to experimental uncertainty and numerical errors.

E. Laser Linewidth Measurement and α Parameter Extraction

The laser linewidth was measured using the homodyne spectrum analysis technique based on the experimental arrangement shown in Fig. 4.

Spectral linewidth measurements can be affected by RIN and laser $1/f$-noise. In the homodyne measurement technique shown in Fig. 4 the autocorrelation of the RIN spectra leads to an approximately constant noise at low frequencies. This noise level depends on the laser injection current and adds to the linewidth spectrum causing broadening of the spectral width.

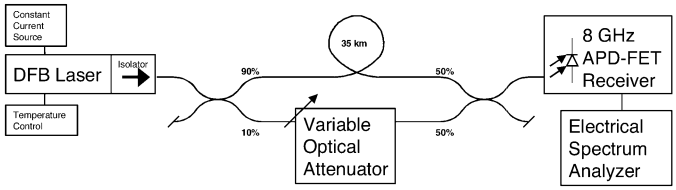

Fig. 4. Experimental arrangement for homodyne linewidth measurement.

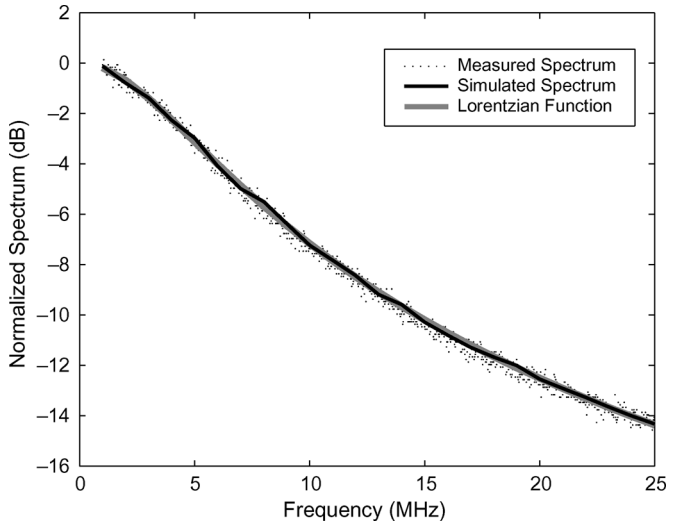

Fig. 5. Comparison between simulated spectrum ($\alpha = 1.55$) with measured spectrum from the homodyne measurement technique.

The $1/f$-noise which is power independent may also affect the linewidth measurement resulting in a residual linewidth at high power levels [23]. In our experiments, we have used injection current levels that would give good Lorentzian fits to the spectral linewidth measurements while maintaining the RIN noise at more than 60 dB below the peak signal. In this regime the linewidth measurements were not limited to RIN or laser $1/f$-noise and the expected relationship of spectral linewidth with inverse power of the laser was obtained as discussed in Section IV.

The extracted linewidth enhancement factor α of the DFB laser was found to be 1.55 by comparison of Lorentzian fit parameters to the measured and simulated homodyne spectrum at an injection current $I = 12.9$ mA. The Lorentzian fit was restricted to the frequency range 1–25 MHz such as to avoid $1/f$-noise from the ESA at low frequencies and also RIN noise at higher frequencies. Fig. 5 shows the comparison between the measured and simulated spectrum of the DFB laser for $\alpha = 1.55$. Both spectra followed a Lorentzian function as also shown in Fig. 5. The simulated spectrum was obtained by taking the Fourier transform of two interfering electric fields, one being a delayed replica of the other, for the homodyne technique. The normalized complex electric field $E(t)$ is expressed as [7]

$$E(t) = \sqrt{S(t)}e^{j(\omega t + \theta(t))} \tag{26}$$

such that the absolute square of this field amplitude corresponds to the photon number. The numerical simulation technique to obtain $S(t)$ and $\theta(t)$ is described in Section IV using the extracted parameters in Table I.

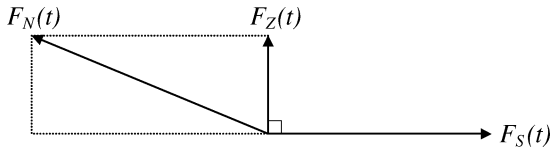

Fig. 6. Schematic representation of the mutual correlations among the functions $F_S(t)$, $F_N(t)$, and $F_Z(t)$. The vector $F_Z(t)$ is orthogonal to $F_S(t)$.

IV. Simulation Results and Discussion

A. Noise Generation Technique

Obtaining the explicit form for each of the functions $F_S(t)$, $F_N(t)$, and $F_\theta(t)$ is necessary to perform numerical integration of (1)–(3). If these noise sources are not cross correlated, we could numerically simulate them with three independent white Gaussian random variables. However, because of the cross correlated relation between S and N expressed in (10), we define a new variable $F_Z(t)$ such that

$$F_Z(t) = F_S(t) + F_N(t) \tag{27}$$

to simultaneously generate the cross correlated noise sources $F_S(t)$ and $F_N(t)$. The idea of orthogonalization of the functions is illustrated in Fig. 6 [24]. The noise functions $F_S(t)$ and $F_Z(t)$ are mutually orthogonal without cross correlations between them so that we can define them independently and hence obtain $F_N(t)$ from (27).

From (6) to (8) and (10) to (12), the auto and cross correlations of the new random function $F_Z(t)$ are

$$\langle F_Z(t)F_Z(t')\rangle = 2D_{ZZ}\delta(t-t') \tag{28}$$
$$\langle F_Z(t)F_S(t')\rangle = 0 \tag{29}$$
$$\langle F_Z(t)F_\theta(t')\rangle = 0 \tag{30}$$

with

$$2D_{ZZ} = \frac{2N(t)}{\tau_n}. \tag{31}$$

The delta functions appearing in (6) and (28) are treated in the numerical calculation such that

$$\langle F_i(t)F_j(t')\rangle = \begin{cases} \frac{2D_{ij}}{\Delta t}, & \text{for } |t-t'| < \frac{1}{2}\Delta t \\ 0, & \text{for } |t-t'| > \frac{1}{2}\Delta t \end{cases} \tag{32}$$

where Δt is the sampling time interval. Since S, N, and θ vary with time, D_{ij} (with i and j standing for any S, N, θ, or Z) in (7)–(10) and (31) also vary with time.

The noise sources are expressed as

$$F_S(t) = \sqrt{\frac{2D_{\mathrm{SS}}(t)}{\Delta t}} \cdot x_s \tag{33}$$
$$F_\theta(t) = \sqrt{\frac{2D_{\theta\theta}(t)}{\Delta t}} \cdot x_\theta \tag{34}$$
$$F_Z(t) = \sqrt{\frac{2D_{ZZ}(t)}{\Delta t}} \cdot x_z \tag{35}$$
$$F_N(t) = F_Z(t) - F_S(t) \tag{36}$$

where x_s, x_θ, and x_z are three independent random numbers taken from a Gaussian distribution with zero mean values and unity variances.

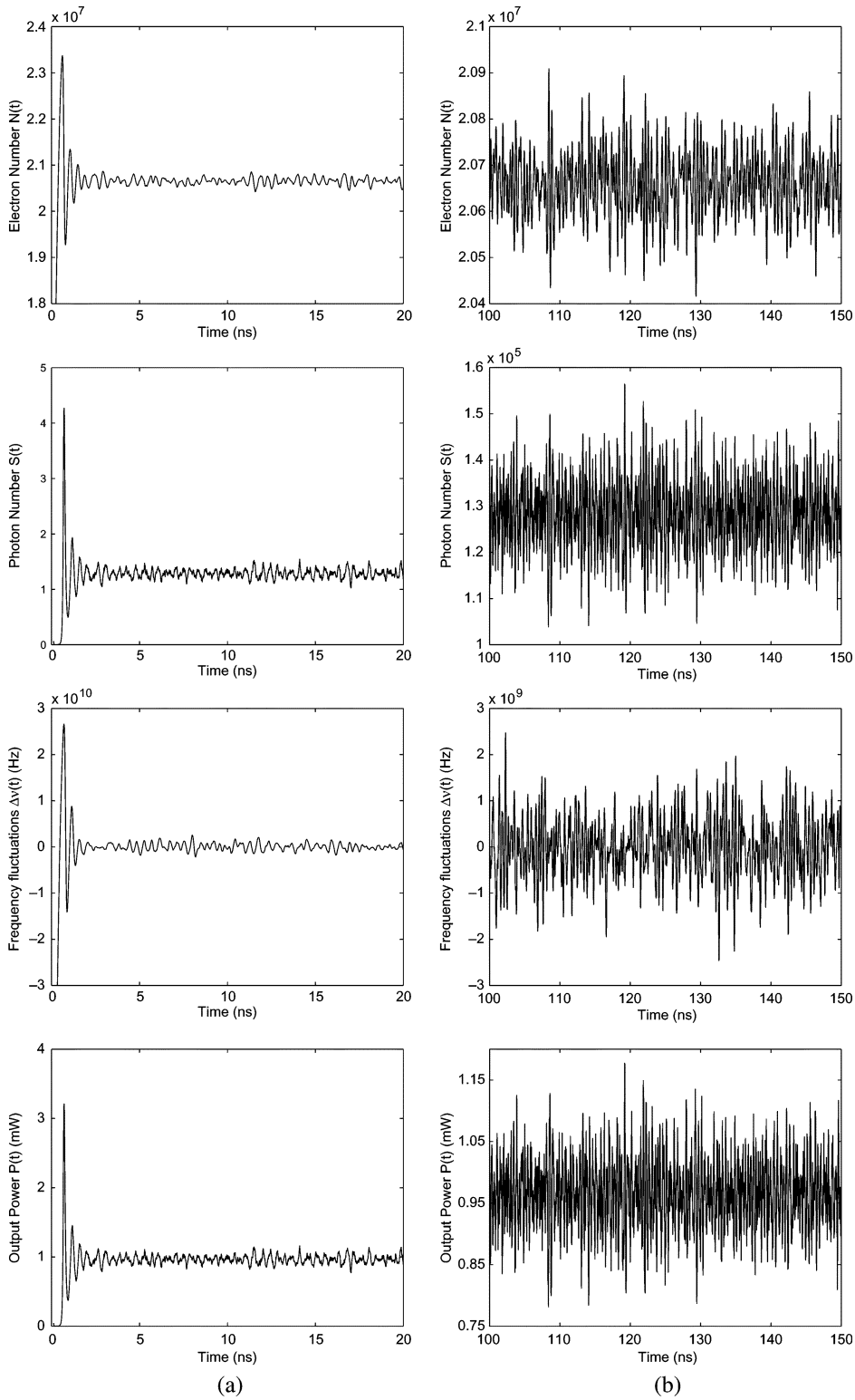

Fig. 7. Simulated time variations of the carrier number $N(t)$, photon number $S(t)$, instantaneous frequency fluctuations $\Delta\nu(t)$, and output power $P(t)$. (a) During transients. (b) After termination of transients.

B. Carrier Number, Photon Number, Frequency Shift, and Power Results

Numerical results for the carrier number $N(t)$, photon number $S(t)$, instantaneous frequency shift $\Delta\nu(t)$, and output power $P(t)$ were obtained using the extracted parameters found in Section III for the DFB laser. The fourth-order Runge–Kutta method using a short interval of $\Delta t = 10$ ps was used to carry out the numerical integrations of (1)–(3). This small value of Δt results in noise sources that approximately describe a white noise spectrum up to a frequency of 100 GHz $(= 1/\Delta t)$, which is much higher than the relaxation frequency (5.3 GHz at an injection current level of 26.3 mA).

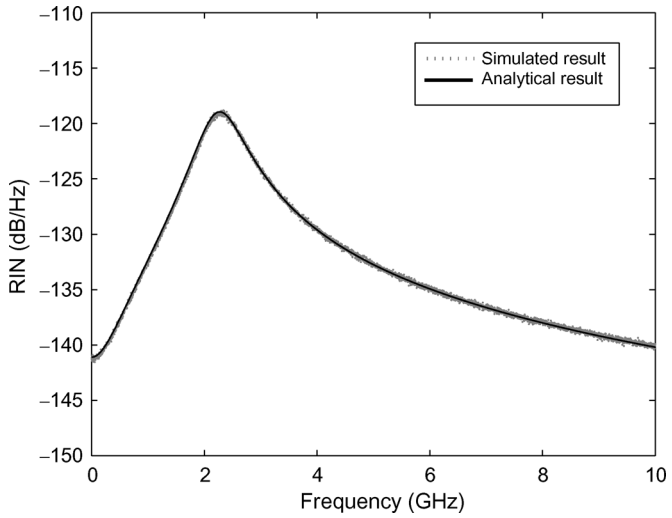

Fig. 8. Simulated RIN spectrum of the laser diode at an injection current $I = 12.9$ mA. The analytical result is also shown for comparison.

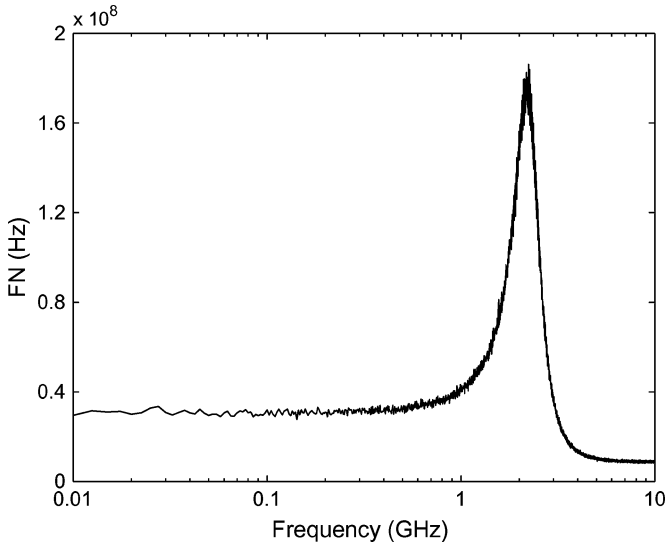

Fig. 9. Simulated FN spectrum of the laser diode at an injection current $I = 12.9$ mA.

The time evolution of the carrier number $N(t)$, photon number $S(t)$, frequency fluctuations $\Delta\nu(t)$, and output power $P(t)$ during and after the termination of transients are plotted in Fig. 7(a) and (b), respectively, at an injection current $I = 12.9$ mA. From Fig. 7, it is readily seen that adding the noise operators causes a fluctuation of these physical quantities around their steady-state values during and after the transient period. The effect of noise is less visible during the start-up transient, due to the relative scale of the transient conditions and noise.

C. Intensity Noise, Frequency Noise, and Linewidth

Simulations of RIN and frequency, or phase, noise (FN) of the laser are evaluated from fluctuations $\delta P(t)$ and $\Delta\nu(t)$, respectively, that result from time integration of (1)–(3) and using (4) and (13). The spectra of the RIN and FN are calculated, using the fast Fourier transform, over a time period T from the equations [24]

$$\mathrm{RIN} = \frac{1}{\langle P\rangle^2}\left\{\frac{1}{T}\left|\int_0^T \delta P(\tau)e^{-j\omega\tau}d\tau\right|^2\right\} \tag{37}$$

$$\mathrm{FN} = \frac{1}{T}\left|\int_0^T \Delta\nu(\tau)e^{-j\omega\tau}d\tau\right|^2 \tag{38}$$

where ω is the angular frequency. Fig. 8 shows the simulated RIN spectrum at an injection current $I = 12.9$ mA. The analytical solution from (16) is also shown on the figure for comparison. The effect of transients on calculations is avoided by counting the fluctuations after $t = 100$ ns. The laser RIN is maximum around the relaxation oscillation frequency for injection currents near threshold and drops off at higher injection currents. The RIN varies approximately between -145 and -115 dB/Hz.

Fig. 9 shows the FN characteristics of the laser diode. The FN spectrum is relatively flat at low frequencies and peaks at the relaxation oscillation frequency. The laser linewidth, the full-width at half-maximum (FWHM) of the single-mode spectrum, is determined from the low-frequency component of the FN as [25]

$$\Delta f = \frac{\mathrm{FN}(0)}{2\pi}. \tag{39}$$

Frequency noise simulation at very low frequencies is necessary for characterization of the linewidth Δf. Although this is very difficult when using the short integration step $\Delta t = 10$ ps from the computational point of view, the flatness of the FN at low-frequency side enabled us to approximately calculate Δf. The calculated value at the injection current $I = 12.9$ mA is $\Delta f = 4.9$ MHz.

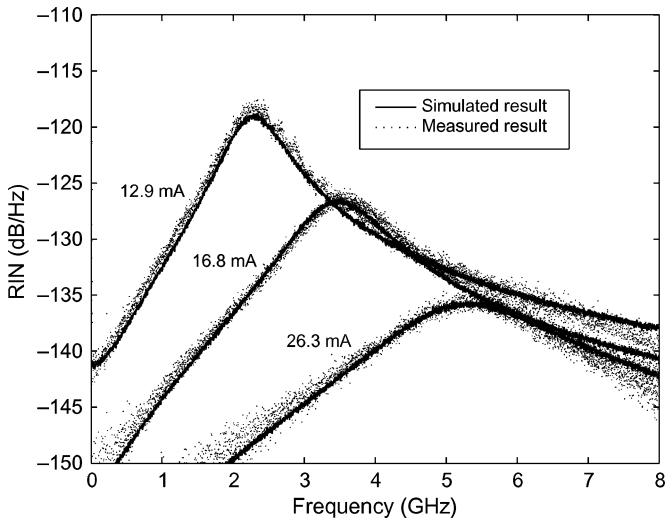

Fig. 10. Comparison of simulated with measured RIN spectra for the DFB laser at different injection current levels.

D. Comparison of Simulated RIN and Linewidth with Experiments

Simulations of the RIN and linewidth Δf, calculated from the FN spectra, are compared in Figs. 10 and 11, respectively, with

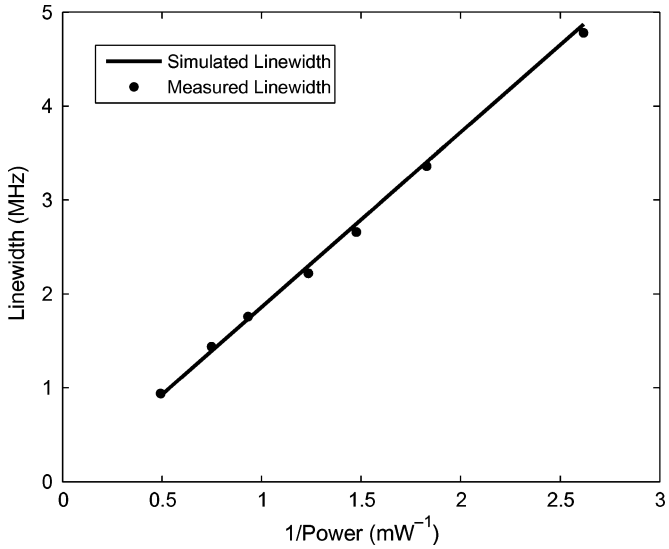

Fig. 11. Comparison of simulated spectral linewidth versus inverse power with measured results for the DFB laser.

measured data for the laser diode. Generally, the linewidth Δf decreases as the laser power increases [26] and the simulated linewidth as a function of inverse power is in agreement with the measured results as shown in Fig. 11 for injection current levels ranging from 12.9 to 25.0 mA. As can be seen from Fig. 11 the linewidth measured is not limited by $1/f$-noise of the laser even at the highest power level. The linewidth–power product, $\Delta f \cdot P$, of the DFB laser is found to be 1.9 MHz $\cdot$ mW. Similar agreement for the RIN spectra at different injection current levels is observed with measured data, as shown in Fig. 10, proving the robustness of the parameter extraction procedure and accuracy of the model.

V. Conclusion

Numerical simulations of intensity and phase noise for semiconductor lasers are demonstrated. The noise effects are analyzed through the study of RIN, FN, and the linewidth Δf of the laser. The rate equations in the laser model are presented in a form containing only parameters that can be extracted from measurements. The extraction procedure to obtain the parameters is based on measurements of the RIN frequency spectra and the linewidth of the laser diode, and simple curve fitting. The agreement between measured and simulated data at different injection current levels for the RIN and linewidth Δf of the DFB laser has proven the accuracy of the proposed extraction method and the simulation technique used to generate the noise effects. The extracted parameters, which accurately reproduced the measured results for intensity and phase noise, are suitable for the purpose of system simulations.

References

[1] S. Mohrdiek, H. Burkhard, F. Steinhagen, H. Hillmer, R. Losch, W. Schlapp, and R. Gobel, "10-Gb/s standard fiber transmission using directly modulated 1.55-μm quantum-well DFB lasers," *IEEE Photon. Technol. Lett.*, vol. 7, no. 11, pp. 1357–1359, Nov. 1995.

[2] P. A. Morton, T. Tanbun-Ek, R. A. Logan, D. A. Ackerman, G. Shtengel, N. Chand, J. E. Johnson, R. D. Yadvish, M. Sergent, and P. F. Sciortino, Jr., "High-speed, low chirp, directly modulated 1.55 μm DFB laser sources for 10 Gbit/s local distribution," presented at the Opt. Fiber Commun., San Jose, CA, 1996, Paper TuH6, unpublished.

[3] E. Mortazy, V. Ahmadi, and M. K. Moravvej-Farshi, "An integrated equivalent circuit model for relative intensity noise and frequency noise spectrum of a multimode semiconductor laser," *IEEE J. Quantum Electron.*, vol. 38, no. 10, pp. 1366–1371, Oct. 2002.

[4] P. Andrekson and P. Andersson, "Parasitic element influence on the wideband electrical noise and modulation response of semiconductor lasers," *IEEE J. Quantum Electron.*, vol. QE-23, no. 6, pp. 1048–1053, Jun. 1987.

[5] K. Czotscher *et al.*, "Intensity modulation and chirp of 1.55- μm multiple-quantum-well laser diodes: modeling and experimental verification," *IEEE J. Sel. Topics Quantum Electron.*, vol. 5, no. 3, pp. 606–612, May-Jun. 1999.

[6] P. André, A. Teixeira, L. P. Pellegrino, M. Lima, R. Nogueira, P. Monteiro, A. N. Pinto, J. L. Pinto, and J. F. D. Rocha, "Extraction of laser parameters for simulation purposes," presented at the NUSOD'05, Berlin, Germany, 2005, paper WP19.

[7] K. Petermann, *Laser Diode Modulation and Noise*. Norwell, MA: Kluwer, 1988, ch. 2.

[8] R. Tucker and D. J. Pope, "Circuit modeling of the effect of diffusion on damping in a narrow-stripe semiconductor laser," *IEEE J. Quantum Electron.*, vol. QE-19, no. 7, pp. 1179–1183, Jul. 1983.

[9] R. Tucker and I. P. Kaminow, "High-frequency characteristics of directly modulated InGaAsP ridge waveguide and buried heterostructure lasers," *J. Lightw. Technol.*, vol. LT-2, no. 4, pp. 385–393, Aug. 1984.

[10] J. C. Cartledge and R. C. Srinivasan, "Extraction of DFB laser rate equation parameters for system simulation purposes," *J. Lightw. Technol.*, vol. 15, no. 5, pp. 852–860, May 1997.

[11] J. Gao, X. Li, J. Flucke, and G. Boeck, "Direct parameter-extraction method for laser diode rate-equation model," *J. Lightw. Technol.*, vol. 22, no. 6, pp. 1604–1609, Jun. 2004.

[12] R. Tucker, "High-speed modulation of semiconductor lasers," *J. Lightw. Technol.*, vol. 3, no. 12, pp. 1180–1192, Dec. 1985.

[13] T. L. Koch and R. A. Linke, "Effect of nonlinear gain reduction on semiconductor laser wavelength chirping," *Appl. Phys. Lett.*, vol. 48, pp. 613–615, 1986.

[14] G. P. Agrawal, "Spectral hole-burning and gain saturation in semiconductor lasers," *J. Appl. Phys.*, vol. 63, pp. 1232–1234, 1988.

[15] A. Tomita and A. Suzuki, "A new density matrix theory for semiconductor lasers, including non-Markovian intraband relaxation and its application to nonlinear gain," *IEEE J. Quantum Electron.*, vol. 27, no. 6, pp. 1630–1641, Jun. 1991.

[16] B. R. Clarke, "The effect of reflections on the system performance of intensity modulated laser diodes," *J. Lightw. Technol.*, vol. 9, no. 6, pp. 741–749, Jun. 1991.

[17] G. P. Agrawal and N. K. Dutta, *Semiconductor Lasers*. New York: Van Nostrand Reinhold, 1993.

[18] C. Henry, "Theory of the phase noise and power spectrum of a single mode injection laser," *IEEE J. Quantum Electron.*, vol. QE–19, no. 9, pp. 1391–1397, Sep. 1983.

[19] D. Derickson, *Fiber Optic Test and Measurement*. Englewood Cliffs, NJ: Prentice-Hall, 1998.

[20] K. Y. Lau and A. Yariv, "Ultra-high speed semiconductor lasers," *IEEE J. Quantum Electron.*, vol. QE–21, no. 9, pp. 121–138, Sep. 1985.

[21] M. C. Cox, N. J. Copner, and B. Williams, "High sensitivity precision relative intensity noise calibration standard using low noise reference laser source," *Proc. Inst. Elect. Eng. Sci. Meas. Technol.*, vol. 145, no. 4, pp. 163–165, 1998.

[22] G. E. Obarski and J. D. Splett, "Transfer standard for the spectral density of relative intensity noise of optical fiber sources near 1550 nm," *J. Opt. Soc. Amer. B*, vol. 18, no. 6, pp. 750–761, 2001.

[23] K. Kikuchi, "Effect of 1/f-type FM noise on semiconductor laser linewidth residual in high-power limit," *IEEE J. Quantum Electron.*, vol. 24, no. 6, pp. 684–688, Jun. 1989.

[24] M. Ahmed, M. Yamada, and M. Saito, "Numerical modeling of intensity and phase noise in semiconductor lasers," *IEEE J. Quantum Electron.*, vol. 37, no. 12, pp. 1600–1610, Dec. 2001.

[25] S. Ghoniemy, L. MacEachern, and S. Mahmoud, "Analytical expressions, modeling, and simulations of intensity and frequency fluctuations in directly modulated semiconductor lasers," *Opt. Eng.*, vol. 43, pp. 224–233, 2004.

[26] G. Arnold, K. Petermann, and E. Schlosser, "Spectral characteristics of gain-guided semiconductor lasers," *IEEE J. Quantum Electron.*, vol. QE-19, no. 6, pp. 974–980, Jun. 1983.

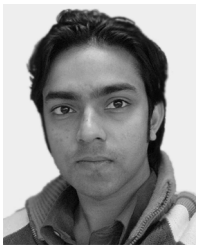

Irshaad Fatadin (M'02) received the B.Sc. degree (hons.) in physics from the University of Delhi, Delhi, India, in 2000, and the M.Phil. degree in microelectronic engineering and semiconductor physics from the University of Cambridge, Cambridge, U.K., in 2002.

He is a Higher Research Scientist in the Photonics Group at the National Physical Laboratory, Middlesex, U.K. His research and development interests include the areas of laser physics, optical amplifiers, optical waveguides, photonic integration, optical fiber communication systems, and numerical simulation of optoelectronic devices.

Mr. Fatadin is a Chartered Physicist, U.K., and member of the IOP and IEEE Lasers and Electro-Optics Society.

David Ives was born in Burnham-on-Crouch, U.K., in 1967. He received the B.Sc. degree in physics from Birmingham University, Birmingham, U.K., in 1988.

He is a Senior Research Scientist in the Photonics Group at the National Physical Laboratory, Middlesex, U.K. His research and development interests include the areas of optical fiber measurement and characterization, optical fiber test equipment characterization, and numerical simulation of optical communication systems.

Mr. Ives is a Chartered Physicist, U.K., and member of the IOP.

Martin Wicks was born in Stockton-on-Tees, U.K., in 1959. He received the M.A. degree in physics from the University of Cambridge, Cambridge, U.K., in 1981.

He is the Leader of the Photonics Group at the National Physical Laboratory, Middlesex, U.K. The group develops novel measurement methods to support the applications of photonic technologies across a wide range of industry. For many years the group primarily supported the optical telecommunications sector, but in recent years the scope of the research has diversified to reflect the increasing application of photonic technologies to manufacture and the bio and medical sectors. Previously, he worked on the development of optically pumped far infrared lasers and superconducting detectors for frequency metrology.

Mr. Wicks is a Chartered Physicist, U.K., and member of the IOP and Institution of Electric Engineers, U.K.